

Secondary Vertex Finding in Jets with Neural Networks

Jonathan Shlomi¹, Sanmay Ganguly¹, Eilam Gross¹, Kyle Cranmer², Yaron Lipman¹,
Hadar Serviansky¹, Haggai Maron³, Nimrod Segol¹,

¹Weizmann Institute Of Science, Israel

²NYU

³NVIDIA Research

Received: date / Accepted: date

Abstract Jet classification is an important ingredient in measurements and searches for new physics at particle colliders, and secondary vertex reconstruction is a key intermediate step in building powerful jet classifiers. We use a neural network to perform vertex finding inside jets in order to improve the classification performance, with a focus on separation of bottom vs. charm flavor tagging. We implement a novel, universal set-to-graph model, which takes into account information from all tracks in a jet to determine if pairs of tracks originated from a common vertex. We explore different performance metrics and find our method to outperform traditional approaches in accurate secondary vertex reconstruction.

1 Introduction

Identifying jets containing bottom and charm hadrons and separating them from jets that originate from lighter quarks, is a critical task in the LHC physics program, referred to as "flavour tagging". Bottom and charm jets are characterized by the presence of secondary decays "inside" the jet - the bottom and charm hadrons will decay several millimeters past the primary interaction point (primary vertex), and only stable outgoing particles will be measured by the detector. Figure 1 illustrates a typical bottom jet decay, with two consecutive displaced vertices from a bottom decay (blue lines) and charm decay (yellow lines).

Existing flavor tagging algorithms use a combination of low-level variables (the charged particle tracks, reconstructed secondary vertices), and high-level features engineered by experts as input to neural networks of various architectures in order to perform jet flavor classification [1].

Vertex reconstruction can be separated to two tasks, *vertex finding*, and *vertex fitting* [2]. Vertex finding refers to the task of partitioning the set of tracks, and vertex fitting

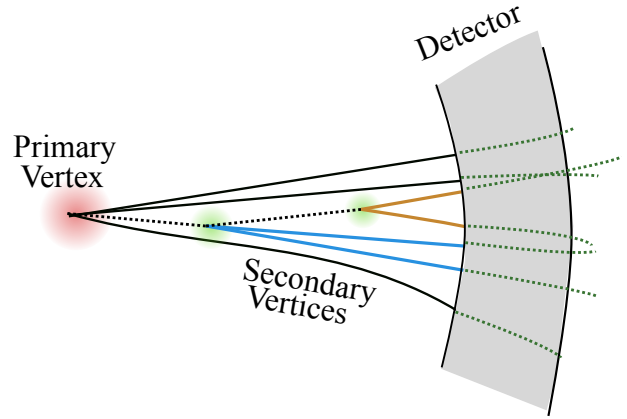


Fig. 1: Illustration of a jet with secondary decay vertices. In order to identify the flavor of the jet, vertex reconstruction aims to group together the tracks measured in the detector based on their point of origin.

refers to estimating the vertex positions given each sub-set of tracks. Existing algorithms typically use an iterative procedure of finding and fitting to perform both tasks together. We focus on using a neural network for vertex finding only. Vertex finding is a challenging task due to two factors:

- Secondary vertices can be in close proximity to the primary vertex, and to each other, within the measurement resolution of the track trajectories.
- The charged particle multiplicity in each individual vertex is low, typically between 1 and 5 tracks.

Vertex reconstruction is in essence an inverse problem of a complicated noisy (forward) function:

$$\text{Particle Decay} \rightarrow \text{Particle Measurement in Detector} \quad (1)$$

Neural networks can find a model for this inverse problem without expert intervention by using supervised learn-

ing, i.e., by providing many examples of the forward process, which can be provided by simulations. They can also be easily optimized by retraining without expert intervention, for example if the pile up conditions change for different periods of data taking.

We first describe the dataset on which we test our proposed algorithm in section 2. The model architecture and the baseline algorithms are described in section 3. Section 4 discusses the performance metrics defined for vertex finding, and the results are presented in section 5. Conclusions are given in section 6.

1.1 Background

Standard Vertex Reconstruction Algorithms. Existing vertex reconstruction techniques are based on the geometry of the tracks, or a combination of the geometry and constraints that are configured by hand to match a specific particle decay pattern [3]. In order to handle finding and fitting multiple vertices, a standard algorithm is Adaptive Vertex Reconstruction (AVR) [2, 4]. The basic concept of AVR is to perform a least squares fit of the vertex position given all the tracks, then remove less compatible tracks from the fit, and refit those tracks again to more vertices. This repeats until no tracks are left.

Deep learning on sets and graphs. Following the successful application of deep learning to images [5, 6], there is an ongoing research effort aimed at applying deep learning to other, differently structured, domains such as unordered sets [7–9] and graphs [10–13]. Typical learning tasks for such domains are point-cloud classification for sets, or molecule property prediction, for graphs. A challenge in both scenarios stems from the arbitrary order of the elements in the set or the nodes in the graph, which hinders the possibility of using simple learning models such as fully connected networks. One popular design principle for networks that process such unordered data is constraining layers to be equivariant or invariant to the reordering operation¹. Recently, the Set2Graph model [14] was proposed as a simple, equivariant model for learning tasks in which the input is an arbitrarily ordered set of n elements and the output is an $n \times n$ matrix that represents their pairwise relations. We use this model in this paper.

Deep learning for particle Physics. Neural networks that operate on sets have been used recently in a number of particle physics applications. The data structure of an unordered

¹If x is an $n \times d$ tensor, and σ is a permutation on n elements, then a layer L is called equivariant if $L(\sigma x) = \sigma L(x)$ and invariant if $L(\sigma x) = L(x)$

set is a natural description for most particle physics reconstruction tasks, and recent progress in the field of graph neural networks [15] has prompted many new applications. For the problem of track reconstruction, a graph neural network was used to classify the paths between adjacent detector "hits" [16]. This is a similar application to vertex finding since the end result must be a partition of the set of hits to different tracks. Direct jet classification has also been proposed with a few different variants of message passing networks [17–20].

2 Data

We test the proposed algorithm on a simulated dataset. The dataset consists of jets sampled from $pp \rightarrow t\bar{t}$ events at $\sqrt{s} = 14$ TeV. The events are generated with PYTHIA8 [21] and a basic detector simulation is performed with DELPHES [22], emulating a detector similar to ATLAS [23]. charged particle tracks are represented by 6 perigee parameters ($d_0, z_0, \phi, \cot\theta, p_T, q$) and their covariance matrix. Noise is added to the track perigee parameters with gaussian smearing. The track parameters resolution depends on the transverse momentum, p_T and pseudo-rapidity η of the track, in a qualitatively similar way to the measurements reported in [23]. The covariance matrix is diagonal in this simplified track smearing model.

Jets are constructed from calorimeter energy deposits with the anti- k_T algorithm [24] with a distance parameter of $R = 0.4$. Charged tracks are cone associated to jets with a $\Delta R < 0.4$ cone around the jet axis. The flavor labeling of jets (as bottom, charm or light) is done by matching weakly decaying bottom and charm hadrons to the jet with a ΔR cone of size 0.3.

A basic jet selection is applied, requiring jets with $p_T > 20$ GeV, and $|\eta| < 2.5$. The input to the vertex finding algorithms is the set of tracks associated to each jet, and the jet 4 vector. The jet 4 vector is described by p_T, η, ϕ and the jet mass.

Dataset Composition. The properties of secondary vertices, such as their distance from the primary vertex, depend on the jet flavor but also on p_T, η , and number of tracks. However, the distribution of those parameters is different for the different flavors, depending on the process used to generate the sample. The dataset is therefore built by sampling equal numbers of jets from each flavor in each $(p_T, \eta, n \text{ tracks})$ bin, as illustrated in figure 2a. For each bin, the flavor with the least amount of jets (usually c-jets) in that bin determines the number of jets from the other flavors that are sampled. Figure 2b shows the resulting distribution of number of vertices in each jet flavor, and figure 2c shows the distribution of p_T, η , and number of tracks for all the flavors. The dataset

is split to training (500K jets), validation and testing datasets (100K jets each).

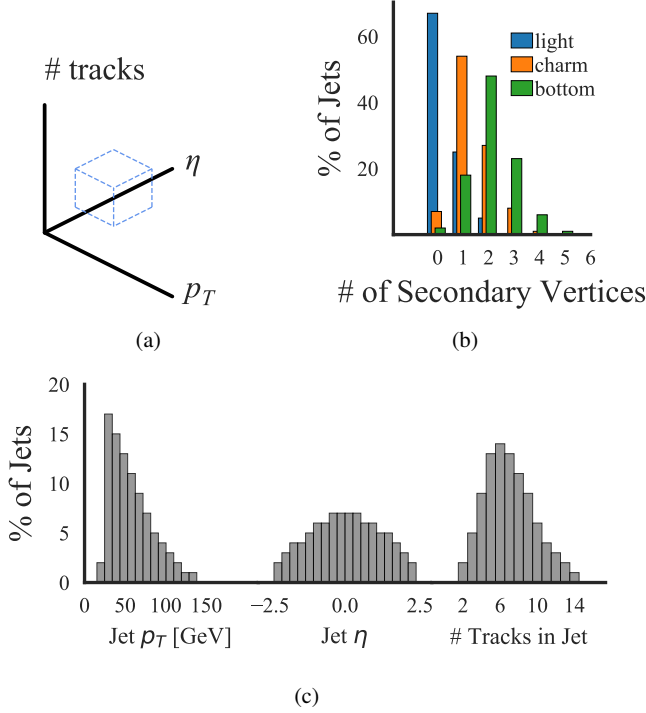


Fig. 2: (a) the dataset is composed by selecting equal numbers of jets from each flavor in each bin of p_T , η , and number of tracks. (b) Distribution of the number of secondary vertices for the different jet flavors. (c) The resulting distribution of p_T , η , and number of tracks in the dataset.

3 Vertex Finding Algorithms

We compare 3 different algorithms.

- Adaptive Vertex Reconstruction (AVR).
- Set to Graph neural network (S2G).
- Track Pair classifier (TP).

AVR serves as the baseline, and represents the existing vertex reconstruction algorithms. The S2G and TP algorithms are neural networks. The architectures of both models are described below.

3.1 Adaptive Vertex Reconstruction

We use adaptive vertex reconstruction as implemented in the RAVE software package [4]. This algorithm is a representative of existing (non neural network based) methods. The input to the algorithm is the set of tracks associated to the

jet and their covariance matrix. The output is a set of vertices, and a set of track-to-vertex association weights (The algorithm can associate a track to more than one vertex). To convert this output into an unambiguous partition, each track is assigned to the vertex to which it has the highest weight. There are hyper-parameters that control the iterative fitting/finding procedure such as cuts on track-to-vertex weight for removing outliers, and these were scanned to find the most performant set of cuts based on the Rand Index (defined in section 4.1). Additional details about the hyper-parameter optimisation is given in Appendix A.

3.2 Set-to-Graph Neural Network

For the neural network training, the vertex finding task is cast to an edge classification task, as illustrated in figure 3. The input is the tracks associated to a jet, represented as an array of $n_{\text{tracks}} \times d_{\text{in}}$, with the $d_{\text{in}} = 10$ features composed of the 6 track perigee parameters and the jet 4-vector (the jet features are duplicated for each track). The output is a 0/1 label attached to each pair of tracks indicating if they originated from the same position in space or not.

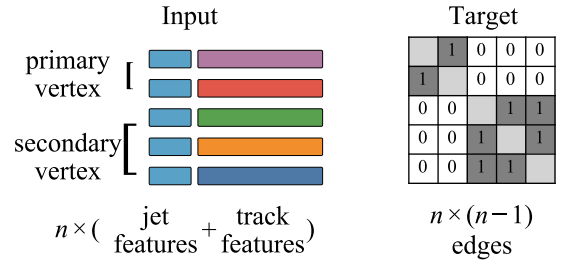


Fig. 3: The input and training target for the neural network algorithms. For a jet with n tracks, the input is an array of $n \times d_{\text{in}}$ track and jet features (jet features are represented by the light blue boxes, track features by the colored boxes), and the target output is a binary classification label for each of the $n \times (n-1)$ ordered pairs of tracks in the jet.

The Set to Graph (S2G) network is built as a composition of 3 modules, $\psi \circ \beta \circ \phi$: A set-to-set component ϕ , a broadcasting layer β and a final edge classifier ψ . Here we give only a high level description of what each module does and its purpose, the specific model details are given in Appendix B. The model architecture is illustrated in figure 4.

The set-to-set component ϕ takes as input the array of size $n_{\text{tracks}} \times d_{\text{in}}$. The output of ϕ is a hidden representation vector for each track, with size $n_{\text{tracks}} \times d_{\text{hidden}}$. ϕ is where information is exchanged between tracks, it is implemented as a DeepSet [7] network.

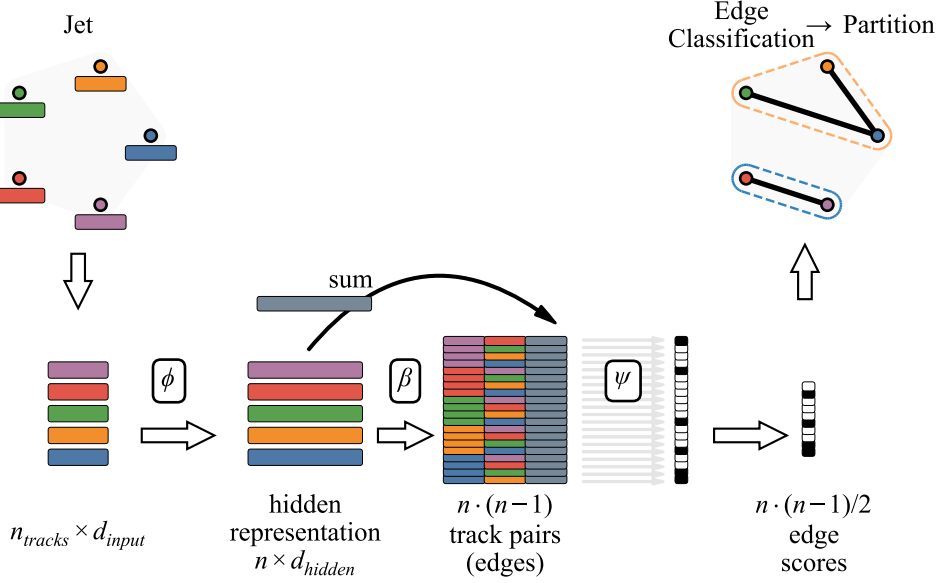


Fig. 4: Partitioning a set of jet tracks using a neural network. A set-to-set component, ϕ , creates a hidden representation of each track, with size d_{hidden} . A broadcasting layer β , then creates a representation for each directed edge (ordered pair of tracks in the jet) by combining the representation of the two tracks and the sum of all representations. An edge classifier ψ then operates on the directed edges. This output is used for training the model (see the target definition in figure 3). During inference the output of the edge classifier is symmetrized to produce an edge score. Edges whose score is over a threshold are classified as connected. The connected components of the resulting graph are used to define the set partition.

The broadcasting layer β constructs a representation for each ordered pair of tracks (directed edge) using the output of ϕ . The edge representation is simply a concatenation of the representation of the two tracks, with the sum of all track representations, resulting in an output of size $n \cdot (n - 1) \times d_{\text{hidden}} \cdot 3$.

The edge classifier ψ is an MLP which operates on the edges to produce an edge score. This edge score is trained according to the target defined in figure 3. During inference (after the training is complete) the edge scores are symmetrized, so for an unordered track pair the edge score is:

$$\text{Edge score} = \psi(\text{track}_i, \text{track}_j) + \psi(\text{track}_j, \text{track}_i) \quad (2)$$

A sigmoid function is applied to this score to give the probability the track pair originated from the same vertex.

To compute the vertex finding performance metrics (defined in section 4.2) the network output is converted into a cluster assignment. track-pairs whose probability is above a threshold of 0.5 are considered connected, turning the set of input tracks into a graph of connected nodes. Connected elements in the resulting graph are grouped together to form the cluster assignment.

3.3 Track Pair Classifier

The Track Pair (TP) classifier serves as a baseline neural network algorithm that will allow us to quantify the contribution of the information exchange between tracks to the overall vertex finding performance. We expect that being aware of all tracks is important for the performance, as the probability of a track pair being connected is conditional on the presence or lack of additional tracks nearby. This algorithm is still expected to perform reasonably well, as it can still learn to join together tracks based on their geometry alone.

The TP classifier shares the same architecture of $\psi \circ \beta \circ \phi$ as the S2G model, with two modifications. First, the DeepSet based ϕ layer is replaced by an MLP applied to each track in the jet (independently from the other tracks) to produce some hidden vector representation of that track. This is illustrated in figure 5.

Theoretically, it was recently proven [25] that the DeepSets module has maximal equivariant expressive power and can approximate arbitrary continuous equivariant functions of sets, in contrast to an MLP acting separately on each input track.

Second, the broadcasting layer β does not use the sum of the track hidden representations. The ψ network operates only on the pair of track hidden representations. Therefore in

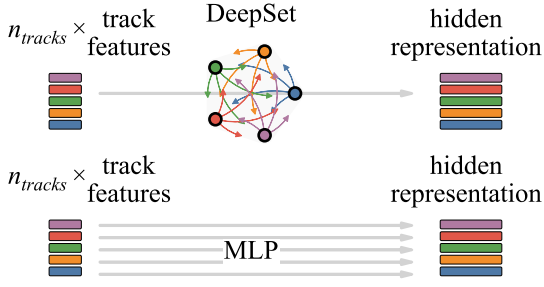


Fig. 5: The DeepSet module ϕ in the S2G model (top) creates the track hidden representation based on information exchange between the tracks in the jet. The TP classifier (bottom) however, creates the hidden representation with an MLP, which operates on each track individually.

the TP classifier there is no information exchange between the track pairs - each track pair is classified independently.

3.4 Training procedure and Loss function

We train the network f to perform edge predictions, i.e., predicting the probability of each pair of input tracks to originate from the same vertex. For a jet with n_{tracks} we therefore predict $n_{tracks} \cdot (n_{tracks} - 1)$ edge scores (We train the network f with the edge predictions before the symmetrization step, which results in $n_{tracks} \cdot \frac{(n_{tracks}-1)}{2}$ edge scores).

In terms of edge classification, it is import to balance the false positive and false negative rates. We initially trained the network with a standard binary cross entropy (BCE) loss:

$$BCE = \sum_{edges} -y_{edge} \cdot \log(\hat{y}_{edge}) - (1 - y_{edge}) \cdot \log(1 - \hat{y}_{edge}) \quad (3)$$

where \hat{y}_{edge} is the edge predicted value, between 0 and 1, and y_{edge} is the truth edge label (0 or 1). The sum is over all edges in a single jet.

Training with BCE loss resulted in a high number of false negatives. We therefore introduced a loss based on the F1 score, defined as:

$$F_1 = \frac{2 \cdot \text{true positives}}{2 \cdot \text{true positives} + \text{false positives} + \text{false negatives}} \quad (4)$$

To compute a differentiable F1 loss, the quantities such as *true positives* are defined as differentiable functions:

$$\begin{aligned} \text{true positives} &\equiv \sum_{edges} \hat{y}_{edge} \cdot y_{edge} \\ \text{false positives} &\equiv \sum_{edges} \hat{y}_{edge} \cdot (1 - y_{edge}) \\ \text{false negatives} &\equiv \sum_{edges} (1 - \hat{y}_{edge}) \cdot y_{edge} \end{aligned} \quad (5)$$

However, training with the F1 score only, was unstable. Given the random weight initialization of the network, the training would sometimes fail to converge. A combined loss of BCE and F1 was finally used:

$$\text{Loss} = BCE - \sum_{jets} F_1 \quad (6)$$

This loss achieved consistent results, and a good balance between false positives and false negatives.

4 Performance Metrics for Vertex Finding

We quantify the vertex finding performance from 3 different "perspectives": The entire jet, individual vertices and pairs of vertices. The motivation for defining multiple metrics is that vertex finding is an intermediate step which is used for a number of other tasks related to event reconstruction. Therefore its important to quantify the performance for a wide variety of jets with different kind of decay topologies.

4.1 Overall Jet Performance

For jets as a whole, we consider the Adjusted Rand Index (ARI) [26]. ARI is a measure of the similarity between two set partitions. For vertex finding where the ground truth is well defined, we can treat the ARI of a jet as a "score" that tells us how well our vertex finding algorithm reproduced the ground truth partition. ARI is a normalized form of the Rand Index, defined as:

$$RI = \frac{\text{number of correct edges}}{\text{number of edges in the set}} \quad (7)$$

Correct edges are edges whose label matches the label they have in the ground truth (true positives and true negatives).

The adjustment of the RI is done by normalizing relative to the expectation value or the RI:

$$ARI = \frac{RI - \mathbb{E}[RI]}{1 - \mathbb{E}[RI]} \quad (8)$$

The expectation value of the RI is defined by a choice of a random clustering model. There are several models one can adopt, described in Ref [27]. In our case a suitable choice is the "one-sided" comparison, where the true vertex assignment is considered fixed, and the expectation value is computed assuming one draws a completely random vertex assignment for the algorithm prediction. The expression for the expectation value is therefore:

$$\mathbb{E}[RI] = \frac{B_{N-1}}{B_N} \frac{\sum_i \binom{g_i}{2}}{\binom{N}{2}} + \left(1 - \frac{B_{N-1}}{B_N}\right) \left(1 - \frac{\sum_i \binom{g_i}{2}}{\binom{N}{2}}\right) \quad (9)$$

where N is the number of tracks in the jet, B_N is the bell number (the number of possible partitions of a set with N elements), the sum is over the i vertices in the jet and g_i is the number of tracks in the i -th vertex.

An ARI score of 1 means the algorithm found the correct cluster assignment, while 0 represents a cluster assignment that is as good as random guessing. We consider the ARI score in 3 categories: perfect - ARI of 1, intermediate - ARI between 0.5 and 1, and poor, lower than 0.5.

4.2 Vertices and Vertex-Pairs Performance

Instead of looking at an entire jet, we can consider subsets of the jet - individual vertices and all possible vertex pairs. We distinguish between *internal*, *external*, and *inter-pair* edges. Figure 6 illustrates the definition. Internal edges connect tracks inside a vertex, Interpair edges connect tracks in one vertex to tracks in the other vertex (this definition is only relevant for vertex pairs), and external edges connect tracks from the vertex/vertex pair to other tracks in the jet. Note that "external edges" refers to edges that are connected only at one end to one of the tracks in the subset under consideration (vertex or vertex pair) - not to all edges that are external to the subset. Considering a specific vertex, or a pair of vertices, we can compute separately the accuracy for each type of edge:

$$\text{Accuracy}_{\text{edge type}} = \frac{\text{correct edges}}{\text{number of edges of that type}} \quad (10)$$

where for internal edges, *correct edges* are those predicted to be connected by the algorithm, and for the other types, correct edges are those predicted to be disconnected.

We can also multiply the different kinds of accuracies to compute an overall accuracy for the vertex/vertex-pair in question ².

For individual vertices, we can evaluate the accuracy as a function of any vertex property we deem important, for example the number of tracks in the vertex. For vertex pairs, an important metric is the performance as a function of the distance between the two vertices. It is expected that as the distance between vertices decreases, accurate vertex finding becomes more difficult, and nearby vertices will be merged. The vertex pair performance metrics allow us to quantify that.

5 Results

The results are summarized in table 1. The S2G model outperforms AVR and TP in all jet performance metrics. The

²For vertices without one kind of edge (e.g vertex with 1 track and no internal edges) the accuracy for that type is set to 1

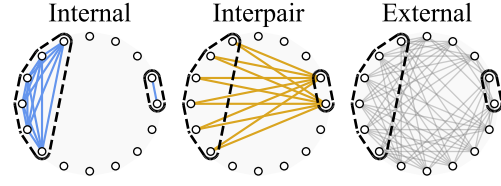


Fig. 6: Definition of internal, external and interpair edges for a pair of vertices.

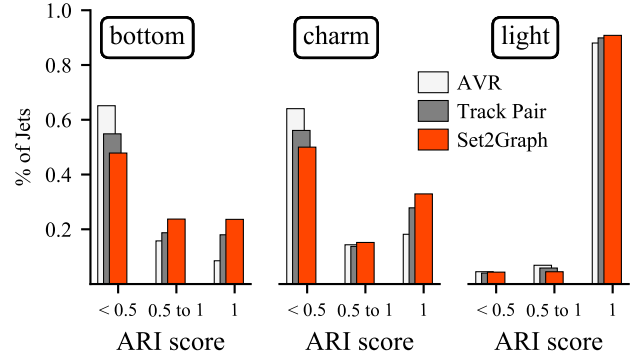


Fig. 7: Adjusted Rand Index scores for the different flavors of jets. We consider 3 categories: *Perfect*- jets with an ARI score of exactly 1, *Intermediate*- a score between 0.5 and 1 and *Poor*- scores below 0.5

improvement is significant (about 20% increase in ARI) for b and c jets, while for light jets the same high performance is maintained. The ARI distribution for the different flavors is shown in figure 7 - while there is still a substantial amount of poorly reconstructed jets (with $\text{ARI} < 0.5$) there are more than twice as many perfectly reconstructed b and c-jets compared to AVR. In figure 8 the mean ARI is shown as a function of both the number of tracks, and the number of vertices in the jet. For b jets, there is a very large improvement in jets with a small number of tracks, but the advantage over AVR is maintained across the entire range. As expected, the track pair classifier matches the S2G performance only in jets with 2 tracks. The AVR algorithm outperforms S2G only in b and c jets which have only one vertex, which are very rare in the dataset.

When considering vertex and vertex-pair metrics, for bottom and charm jets the mean internal accuracy for S2G is within 1% of the baseline, and a large increase (between 10 to 20%) is achieved for external and inter-pair accuracy. Figure 9 shows the performance for vertices, as a function of vertex size (i.e., number of tracks in the vertex). The S2G algorithm maintains an advantage over the full range of vertex sizes - The S2G model has a similar internal accuracy

	Algorithm	Jet			Vertex			Vertex-Pair				
		F1	RI	ARI	internal	external	combined	internal ₁	internal ₂	inter-pair	external	combined
bottom	AVR	0.56	0.61	-0.01	0.91	0.51	0.46	0.59	0.90	0.54	0.58	0.18
	Track Pair	0.61	0.68	0.15	0.93	0.58	0.53	0.60	0.91	0.60	0.62	0.26
	Set2Graph	0.65	0.75	0.34	0.91	0.69	0.62	0.58	0.91	0.70	0.72	0.31
charm	AVR	0.70	0.65	0.22	0.95	0.41	0.39	0.49	0.91	0.49	0.66	0.14
	Track Pair	0.73	0.70	0.33	0.96	0.49	0.46	0.50	0.91	0.57	0.71	0.23
	Set2Graph	0.75	0.73	0.41	0.96	0.56	0.53	0.49	0.92	0.63	0.75	0.25
light	AVR	0.97	0.96	0.93	0.99	0.89	0.88	0.33	0.98	0.73	0.89	0.14
	Track Pair	0.97	0.97	0.94	0.98	0.92	0.91	0.33	0.97	0.86	0.94	0.26
	Set2Graph	0.97	0.97	0.94	0.98	0.93	0.91	0.33	0.98	0.87	0.95	0.26

Table 1: Vertex finding performance. See section 4 for the definitions of the various metrics.

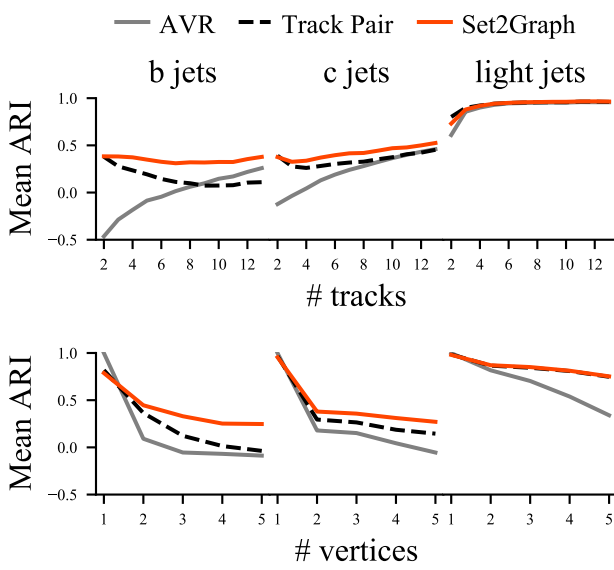


Fig. 8: Mean Adjusted Rand Index scores for the different flavors of jets as a function of the jet properties.

to the baseline, but a 10% increase in external accuracy for smaller vertices.

Figure 10 show the performance for vertex pairs, as a function of the distance between the vertices. Again the S2G shows a promising ability to separate vertices even when the distance between them approaches 0. The performance increase of about 10% in combined accuracy comes from the improvement in interpair and external accuracy, i.e., less merging of vertices.

The TP algorithm has a lower ARI by about 10% compared to the S2G model. This shows that, as expected, the S2G network incorporates global track information to produce more accurate edge predictions.

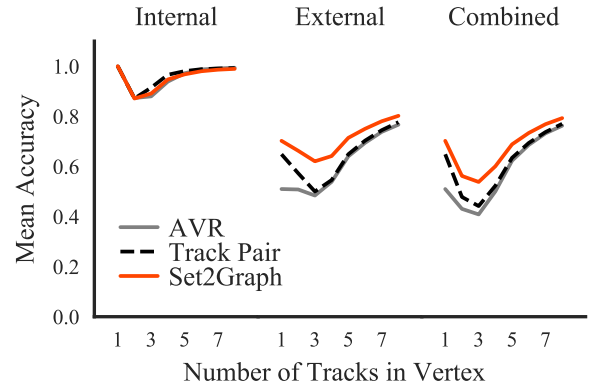


Fig. 9: Vertex performance as a function of the vertex size. Internal, external and combined accuracy are defined in section 4.2

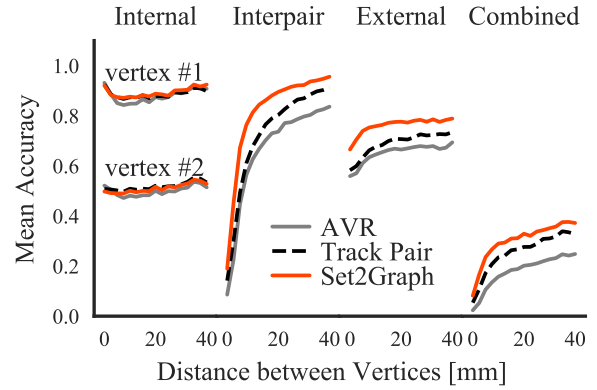


Fig. 10: Vertex pair accuracy as a function of distance between the vertices. The internal accuracy is shown for both smaller vertex (the vertex with fewer tracks, vertex #1) and the larger vertex (vertex #2).

6 Conclusions

We proposed training a neural network to perform vertex finding, using supervised learning. We found that it outperforms standard techniques for multiple performance metrics of vertex reconstruction, and shows promising increase in performance for nearby vertices.

Future work may explore the application of this technique to more complicated decays such as boosted Higgs to (bb/cc), and apply it to more realistic datasets that include full detector simulation and pileup interactions. A particularly critical follow up question is to understand how an increase in the performance metrics defined above, such as ARI, translate to an increase in performance in downstream tasks such as jet flavour classification.

7 Acknowledgments

EG and JS are supported by the NSF-BSF Grant 2017600 and the ISF Grant 125756. This research was partially supported by the Israeli Council for Higher Education (CHE) via the Weizmann Data Science Research Center. KC is supported by the National Science Foundation under the awards ACI-1450310, OAC-1836650, and OAC-1841471 and by the Moore-Sloan data science environment at NYU. HS, NS and YL were supported in part by the European Research Council (ERC Consolidator Grant, "LiftMatch" 771136), the Israel Science Foundation (Grant No. 1830/17) and by a research grant from the Carolito Stiftung (WAIC).

References

1. Daniel Guest, Julian Collado, Pierre Baldi, Shih-Chieh Hsu, Gregor Urban, and Daniel Whiteson. Jet Flavor Classification in High-Energy Physics with Deep Neural Networks. *Phys. Rev.*, D94(11):112002, 2016.
2. Are Strandlie and Rudolf Fruhwirth. Track and vertex reconstruction: From classical to adaptive methods. *Rev. Mod. Phys.*, 82:1419–1458, 2010.
3. G Piacquadio and C Weiser. A new inclusive secondary vertex algorithm for b-jet tagging in ATLAS. *Journal of Physics: Conference Series*, 119(3):032032, jul 2008.
4. Wolfgang Waltenberger. RAVE: A detector-independent toolkit to reconstruct vertices. *IEEE Trans. Nucl. Sci.*, 58:434–444, 2011.
5. Yann LeCun, Léon Bottou, Yoshua Bengio, and Patrick Haffner. Gradient-based learning applied to document recognition. *Proceedings of the IEEE*, 86(11):2278–2324, 1998.
6. Alex Krizhevsky, Ilya Sutskever, and Geoffrey E Hinton. Imagenet classification with deep convolutional neural networks. In *Advances in neural information processing systems*, pages 1097–1105, 2012.
7. Manzil Zaheer, Satwik Kottur, Siamak Ravanbakhsh, Barnabas Poczos, Ruslan R Salakhutdinov, and Alexander J Smola. Deep sets. In *Advances in neural information processing systems*, pages 3391–3401, 2017.
8. Charles R Qi, Hao Su, Kaichun Mo, and Leonidas J Guibas. Pointnet: Deep learning on point sets for 3d classification and segmentation. *Proc. Computer Vision and Pattern Recognition (CVPR), IEEE*, 1(2):4, 2017.
9. Haggai Maron, Or Litany, Gal Chechik, and Ethan Fetaya. On learning sets of symmetric elements. *arXiv preprint arXiv:2002.08599*, 2020.
10. Joan Bruna, Wojciech Zaremba, Arthur Szlam, and Yann LeCun. Spectral Networks and Locally Connected Networks on Graphs. pages 1–14, 2013.
11. Thomas N Kipf and Max Welling. Semi-supervised classification with graph convolutional networks. *arXiv preprint arXiv:1609.02907*, 2016.
12. Justin Gilmer, Samuel S Schoenholz, Patrick F Riley, Oriol Vinyals, and George E Dahl. Neural message passing for quantum chemistry. In *International Conference on Machine Learning*, pages 1263–1272, 2017.
13. Haggai Maron, Heli Ben-Hamu, Nadav Shamir, and Yaron Lipman. Invariant and equivariant graph networks. *arXiv preprint arXiv:1812.09902*, 2018.
14. Hadar Serviansky, Nimrod Segol, Jonathan Shlomi, Kyle Cranmer, Eilam Gross, Haggai Maron, and Yaron Lipman. Set2Graph: Learning Graphs From Sets. *arXiv preprint arXiv:2002.08772*, 2020.
15. Peter W. Battaglia, Jessica B. Hamrick, Victor Bapst, Alvaro Sanchez-Gonzalez, Vinicius Zambaldi, et al. Relational inductive biases, deep learning, and graph networks. *arXiv preprint arXiv:1806.01261*, 2018.
16. Steven Farrell et al. Novel deep learning methods for track reconstruction. In *4th International Workshop Connecting The Dots 2018 (CTD2018) Seattle, Washington, USA, March 20-22, 2018*, 2018.
17. Eric A. Moreno, Olmo Cerri, Javier M. Duarte, Harvey B. Newman, Thong Q. Nguyen, Avikar Periwal, Maurizio Pierini, Aidana Serikova, Maria Spiropulu, and Jean-Roch Vlimant. JEDI-net: a jet identification algorithm based on interaction networks. *Eur. Phys. J.*, C80(1):58, 2020.
18. Huilin Qu and Loukas Gouskos. Jet tagging via particle clouds. *Physical Review D*, 101(5), Mar 2020.
19. J. Bruna K. Cho K. Cranmer G. Louppe et al. I. Henrion, J. Brehmer. Neural message passing for jet physics. In *Deep Learning for Physical Sciences Workshop at the 31st Conference on Neural Information Processing Systems (NIPS)*, 2017.
20. Patrick T. Komiske, Eric M. Metodiev, and Jesse Thaler. Energy flow networks: deep sets for particle jets. *Jour-*

-
- nal of High Energy Physics*, 2019(1), Jan 2019.
21. Torbjörn Sjöstrand, Stefan Ask, Jesper R. Christiansen, Richard Corke, Nishita Desai, Philip Ilten, Stephen Mrenna, Stefan Prestel, Christine O. Rasmussen, and Peter Z. Skands. An introduction to pythia 8.2. *Computer Physics Communications*, 191:159–177, Jun 2015.
 22. J. de Favereau, C. Delaere, P. Demin, A. Giammanco, V. Lemaître, A. Mertens, and M. Selvaggi. Delphes 3: a modular framework for fast simulation of a generic collider experiment. *Journal of High Energy Physics*, 2014(2), Feb 2014.
 23. G. Aad et al. The ATLAS experiment at the CERN large hadron collider. *Journal of Instrumentation*, 3(08):S08003–S08003, aug 2008.
 24. Matteo Cacciari, Gavin P. Salam, and Gregory Soyez. The anti- k_t jet clustering algorithm. *JHEP*, 04:063, 2008.
 25. Nimrod Segol and Yaron Lipman. On universal equivariant set networks. *arXiv preprint arXiv:1910.02421*, 2019.
 26. Lawrence Hubert and Phipps Arabie. Comparing partitions. *Journal of Classification*, 2(1):193–218, December 1985.
 27. Alexander Gates and Yong-Yeol Ahn. The impact of random models on clustering similarity. *Journal of Machine Learning Research*, 18, 01 2017.
 28. Maximilian Ilse, Jakub M Tomczak, and Max Welling. Attention-based deep multiple instance learning. *arXiv preprint arXiv:1802.04712*, 2018.
 29. Ashish Vaswani, Noam Shazeer, Niki Parmar, Jakob Uszkoreit, Llion Jones, Aidan N Gomez, Lukasz Kaiser, and Illia Polosukhin. Attention is all you need. In *Advances in Neural Information Processing Systems 30*, pages 5998–6008. 2017.
 30. Diederik P Kingma and Jimmy Ba. Adam: A method for stochastic optimization. *arXiv preprint arXiv:1412.6980*, 2014.

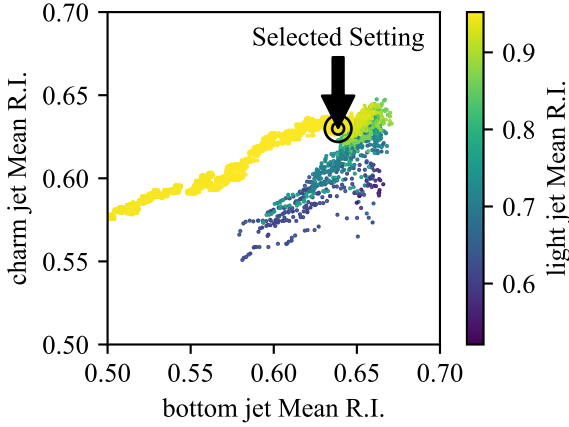


Fig. 11: AVR parameter scan

Appendix A: Hyperparameter Optimization for AVR

The Adaptive Vertex Reconstruction algorithm in Rave [4] has three main parameters that can be adjusted by the user -

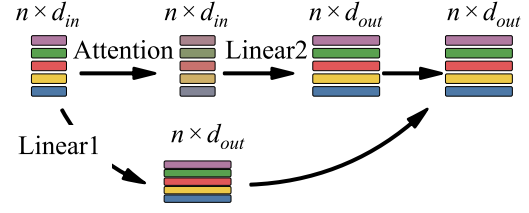
- Primary vertex significance cut
- Secondary vertex significance cut
- minimum weight for a track to stay in a fitted vertex

The values for these parameters were scanned in a grid between 0.1 to 10 for the significance cuts (33 equally spaced values) and between 0.1 to 0.8 for the minimum weight (10 values). For each possible value of the parameters, the mean RI was computed for each of the 3 flavors in the training dataset. The values of the b, c and light jet RI are shown in figure 11. The working point that was chosen had the highest b jet RI with a mean light jet RI above 0.95:

- Primary cut: 2.5
- Secondary cut: 2.5
- minimum weight: 0.2

Appendix B: Model Architecture and Training Details

S2G model. The ϕ component of the S2G model is composed of a sequence of DeepSet layers [7], each of which contain a self-attention mechanism and two linear $d_{in} \rightarrow$

Fig. 12: A single DeepSet layer in the ϕ module.

If we describe the stack of DeepSet layers by their output dimension d_{out} , the ϕ module layer dimensions are:

$$\phi \text{ output dimensions} = (256, 256, 256, 256, 5) \quad (\text{B.2})$$

d_{out} layers, in a structure shown in figure 12. A ReLU non-linearity is used between the layers.

The attention block in the DeepSet layer is a key/query attention [28, 29]:

$$\text{Attention}(X) = \text{softmax} \left(\frac{\tanh f_1(X) \cdot f_2(X)^T}{\sqrt{d_{small}}} \right) \cdot X \quad (\text{B.1})$$

Where X is the $n \times d_{in}$ input, f_1, f_2 are the key and query MLPs of width $d_{small} = d_{in}/10$.

The edge classifier component ψ takes in the $n \cdot (n - 1) \times (5 \cdot 3)$ output of the broadcasting layer, and uses a single hidden layer MLP with output dimensions $(256, 1)$. The edge scores are given by $\psi(\text{track}_i, \text{track}_j) + \psi(\text{track}_j, \text{track}_i)$

Baseline TP Classifier. The MLP that replaces the DeepSet layers has the following output sizes:

$$\phi_{\text{TrackPair}} \text{ output dimensions} = (384, 384, 384, 384, 5) \quad (\text{B.3})$$

The edge classifier component ψ is identical except its input size is now $5 \cdot 2$ instead of $5 \cdot 3$ due to the absence of the sum in the broadcasting layer.

Training Hyperparameters We used a batch size of 2048, Adam optimizer [30] with learning rate of $1e - 3$. Training takes place in less than 2 hours on a single Tesla V100 GPU.